Ultrasonics - Sonochemistry 41 (2018) 252–260

Contents lists available at ScienceDirect

Ultrasonics - Sonochemistry

journal homepage: www.elsevier.com/locate/ultson

Exceptionally high cavitation erosion and corrosion resistance of a high entropy alloy

R.B. Nair[a], H.S. Arora[a], Sundeep Mukherjee[b], S. Singh[c], H. Singh[c], H.S. Grewal[a,*]

[a] Surface Science and Tribology Lab, Department of Mechanical Engineering, Shiv Nadar University, Gautam Budh Nagar, India
[b] Department of Materials Science and Engineering, University of North Texas, Denton, TX 76203, USA
[c] Department of Mechanical Engineering, Indian Institute of Technology Ropar, Rupnagar, India

ARTICLE INFO

Keywords:
Cavitation erosion-corrosion
High entropy alloy
Work-hardening

ABSTRACT

Cavitation erosion and corrosion of structural materials are serious concerns for marine and offshore industries. Durability and performance of marine components are severely impaired due to degradation from erosion and corrosion. Utilization of advanced structural materials can play a vital role in limiting such degradation. High entropy alloys (HEAs) are a relatively new class of advanced structural materials with exceptional properties. In the present work, we report on the cavitation erosion behavior of $Al_{0.1}CoCrFeNi$ HEA in two different media: distilled water with and without 3.5 wt% NaCl. For comparison, conventionally used stainless steel SS316L was also evaluated in identical test conditions. Despite lower hardness and yield strength, the HEA showed significantly longer incubation period and lower erosion-corrosion rate (nearly 1/4th) compared to SS316L steel. Enhanced erosion resistance of HEA was attributed to its high work-hardening behavior and stable passivation film on the surface. The $Al_{0.1}CoCrFeNi$ HEA showed lower corrosion current density, high pitting resistance and protection potential compared to SS316L steel. Further, HEA showed no evidence of intergranular corrosion likely due to the absence of secondary precipitates. Although, the degradation mechanisms (formation of pits and fatigue cracks) were similar for both the materials, the damage severity was found to be much higher for SS316L steel compared to HEA.

1. Introduction

Cavitation erosion is a common mode of material deterioration in hydrodynamic environment. Erosion and corrosion synergy leads to rapid degradation of marine and offshore components such as impellers, ship propellers and valves. During cavitation erosion, material removal takes place due to repetitive impact of micro-jets and shock-waves generated by the implosion of vapour bubbles formed as a result of pressure fluctuations in liquids [1,2]. This leads to severe localized plastic deformation and pitting which eventually causes material failure. Cavitation erosion in corrosive media may further aggravate the degradation process. Different coatings and surface modification techniques have been utilized for improving the cavitation erosion and corrosion resistance of marine components [3–7]. Stainless steels are normally preferred for use in hydraulic systems due to their good corrosion resistance. However, the poor cavitation erosion resistance of stainless steels lowers the working life of the components [8,9]. Advanced materials with superior erosion-corrosion resistance are required to counter such degrading environments.

Recently developed high entropy alloys (HEAs) based on multiple principal elements in equi-molar or nearly equi-molar fractions represent a new paradigm in structural materials [10–13]. Unlike conventional alloys, HEAs are comprised of five or more principle elements with atomic fraction in 5–35% range. HEA may also contain minor elements with atomic fraction typically less than 5%. HEA typically tends to form single-phase solid solution with face centered cubic (FCC), body centered cubic (BCC) and/or hexagonal closed packed (HCP) structure due to their high mixing entropy. According to Gibbs free energy relation, high mixing entropy enhances the phase stability by reducing free energy of the system. Further, the lattice distortions due to increased mixing entropy also results in sluggish diffusion wherein atoms are trapped in low potential energies (LPE) sites. Besides sluggish diffusion, interaction of each constituent elements results in phase transformation due to cocktail effect. It is reported that the sluggish diffusion, severe lattice distortion and cock tail effect results in high corrosion resistance, wear and oxidation resistance and excellent mechanical properties at elevated temperatures [11,14–18]. Although HEAs exhibits high corrosion resistance, however their performance under synergistic cavitation erosion and corrosion has not been explicitly explored. The material's performance under combined erosion

* Corresponding author.
E-mail address: harpreet.grewal@snu.edu.in (H.S. Grewal).

http://dx.doi.org/10.1016/j.ultsonch.2017.09.044
Received 5 June 2017; Received in revised form 19 August 2017; Accepted 25 September 2017
Available online 28 September 2017
1350-4177/

Table 1
Nominal composition of $Al_{0.1}$CoCrFeNi HEA, and SS316L steel used in the current study.

Composition (wt%)	Al	Fe	Cr	C	Mn	Ni	Mo	Co	S	Si	P
$Al_{0.1}$CrCoFeNi HEA	1.2	24.5	22.8	–	–	25.7	–	25.8	–	–	–
SS 316L steel	–	bal.	18	0.035	2	14	3	–	0.03	1	0.045

and corrosion conditions is a function of mechanical properties of material and characteristics of the passive layer. Further the adherence of the passive layer with the substrate also plays an important role in determining the performance of the material under erosion-corrosion conditions. In case of HEAs, stability of passive layer is expectedly high with thickness being limited by sluggish diffusion [19]. However, sustainability and performance of passive layer formed on HEAs under hydrodynamic conditions is not well understood and require detailed investigation.

Among the different compositions, Al_xCoCrFeNi HEA is one of the most widely studied alloy system [20–23]. Wang et al. [21] reported increase in hardness for Al_xCrCoFeNi HEA with an increase in Al content due to the formation of nano scale B_2 and A_2 structure. Tang et al. [24] reported evolution of different phases during annealing of $Al_{0.3}$CrCoFeNi HEA. The formation of $L1_2$ and B_2 phases were related to the reduction in lattice distortion and sluggish diffusion. Laser surface alloyed AlCoCrFeNiTi_2 showed excellent cavitation erosion resistance owing to the presence of ordered B_2 structure [25]. Compared to SS304 steel, AlCrCoFeNi HEA exhibited better cavitation erosion with higher pitting resistance [26]. Further, an increase in Al content in Al_xCrCoFeNi HEA system has been reported to decrease the pitting resistance due to formation of Cr depleted BCC structure [27].

We report on the cavitation erosion and corrosion behavior of $Al_{0.1}$CoCrFeNi high entropy alloy (HEA) and compare with conventionally utilized SS316L stainless steel. $Al_{0.1}$CrCoFeNi HEA showed excellent cavitation erosion-corrosion resistance, which was explained based on its high work-hardening and better pitting resistance compared to SS316L steel.

2. Experimental procedure

For the present study, $Al_{0.1}$CrCoFeNi HEA was selected owing to its high ductility and work-hardening behavior. The alloy was made by vacuum arc melting followed by hot isostatic pressing (HIP) at a pressure of 100 MPa and temperature of 1273 K for 4 h. For comparison, commercially available SS316L steel was used. The nominal composition of $Al_{0.1}$CrCoFeNi HEA and SS316L are shown in Table 1. The microstructure of the HEA and SS316L steel was obtained using electron back-scatter diffraction (EBSD) and X-ray diffraction (XRD). Mechanical properties of both the materials were investigated using micro and nano indentation.

The cavitation erosion tests were conducted using ultrasonic vibratory apparatus (make: Sonics; model VCX 750) in accordance with ASTM G-32 standard. The cavitation erosion testing was performed using indirect method by keeping the sample stationary (Fig. 1). The samples were placed at a distance of 500 μm from the vibrating tip and immersed 10 mm below the free surface. The vibrating tip was operated at a frequency of 20 ± 0.5 kHz with peak-to-peak amplitude of 50 μm.

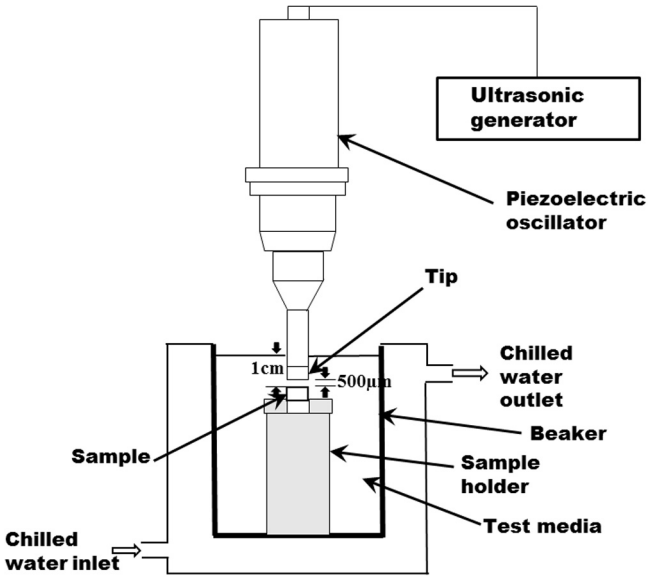

Fig. 1. Schematic illustrating ultrasonication set-up used for cavitation erosion testing.

Test samples were submerged in a 1 litre beaker containing distilled water with (for erosion-corrosion) and without (for pure erosion) 3.5% NaCl solution. The temperature was kept constant at 24 ± 2 °C using cooling coil connected to chiller. Prior to the test, all samples were grounded and polished down to 2000 grit using abrasive paper. Each sample was tested for 20 h with subsequent mass change (0.01 mg) measurements after every one-hour cycle. To ensure repeatability, two samples were tested under each condition. The mass change was converted to corresponding volume loss using the density values shown in Table 2. The results were analysed to determine cumulative volume loss (CVL) and cumulative erosion rate (CER). The morphology of degraded surfaces was analysed using scanning electron microscope (SEM) for evaluation of damage mechanism. The electrochemical corrosion studies comprising tafel and cyclic polarization were performed using potentiostat (make: Gamry, model: 1000E) to determine the corrosion behavior and stability of the passive layer. Tafel tests were performed by varying the potential ± 0.25 V from the open-circuit potential (E_{corr}). Cyclic polarization studies were conducted with maximum current density limited to 10 mA/cm^2. Further the intergranular corrosion testing was also performed using single loop electro-chemical potentio-kinetic reactivation (SL-EPR) test to determine the influence of precipitates on the corrosion behavior.

Table 2
Mechanical and physical properties of $Al_{0.1}$CrCoFeNi high entropy alloy and stainless steel SS316L.

Materials	Density (g/cc)	Hardness H (H_v)	Elastic modulus E (Gpa)	Yield strength σ_y (Mpa)	Ultimate strength, σ_u (Mpa)	Critical fracture strain, ε_f
$Al_{0.1}$CrCoFeNi HEA	7.45	150	186	160	389	0.58
SS316L steel	7.87	226	210	290	580	0.35

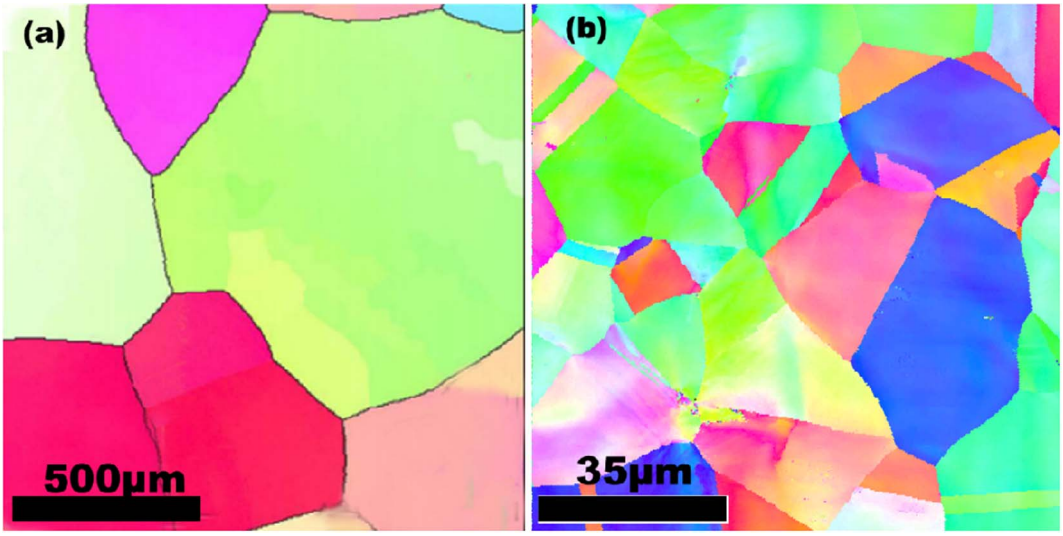

Fig. 2. Electron backscatter diffraction maps for (a) $Al_{0.1}CrCoFeNi$ high entropy alloy [27] and (b) SS316L stainless steel.

3. Result and discussion

3.1. Microstructural characterization

The electron backscatter diffraction (EBSD) results of $Al_{0.1}CrCoFeNi$ HEA and stainless steel (SS316L) are shown in Fig. 2. HEA has an average grain size of several millimetres without any twins [28] while SS316L has an average grain size of about 22 µm along with few twin boundaries. Unusually large grain size for HEA is attributed to the abnormal grain growth during the HIP treatment which was done to reduce porosity in addition to enhancement in ductility. The X-ray diffraction results for $Al_{0.1}CrCoFeNi$ HEA and SS316L steel are shown in Fig. 3. XRD indicates single-phase face cantered cubic (FCC) structure for the HEA. The lattice parameter calculated for the HEA was around 0.358 nm. There was no indication of secondary phase formation, which has been primarily explained by high mixing entropy [12,13]. The increase in the configurational entropy lowers the Gibbs free energy [29], enhancing the stability of solid solution. The configurational entropy (ΔS) is given as [13]:

$$\Delta S_{Conf} = -R\sum_{I=1}^{n} x_i \ln x_i = R\ln n$$

where R is universal gas constant, n is number of elements, and x_i is molar fraction of elements. For $Al_{0.1}CoCrFeNi$ HEA, the configurational entropy was calculated to be around 1.47R, which is higher than that of SS316L steel.

Table 2 shows different mechanical and physical properties of HEA and SS316L steel. Elastic modulus was evaluated from load-displacement curves obtained using nano indentation as shown in Fig. 4. Yield strength and failure strain were obtained from engineering stress-strain curves [30]. Evidently, hardness and elastic modulus of HEA were comparatively lower than SS316L steel. Low hardness of the HEA compared to SS316L steel is due to large grain size of the former. However, significantly large grain size and mild lattice strain of HEA due to low Al fraction, resulted in high ductility (65% higher) as indicated by the fracture strain values.

3.2. Cavitation erosion behaviour

Fig. 5(a) shows the cumulative volume loss as a function of time for $Al_{0.1}CrCoFeNi$ HEA and SS316L under cavitation erosion condition (in distilled water). The HEA showed significantly high cavitation erosion resistance compared to SS316L. After 20 h of testing, cumulative

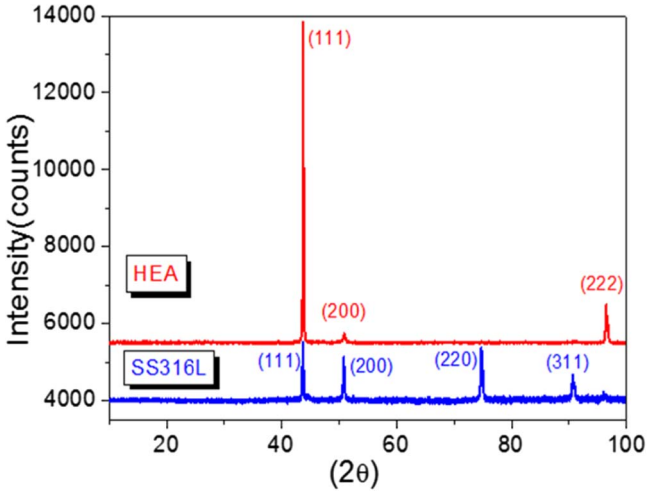

Fig. 3. X ray diffraction (XRD) plots of $Al_{0.1}CrCoFeNi$ high entropy alloy (HEA) and SS316L stainless steel.

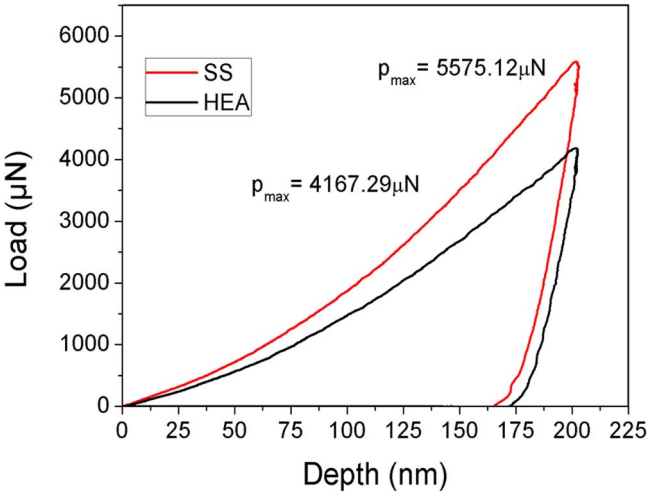

Fig. 4. Load-Displacement plots of $Al_{0.1}CrCoFeNi$ high entropy alloy (HEA) and SS316L stainless steel.

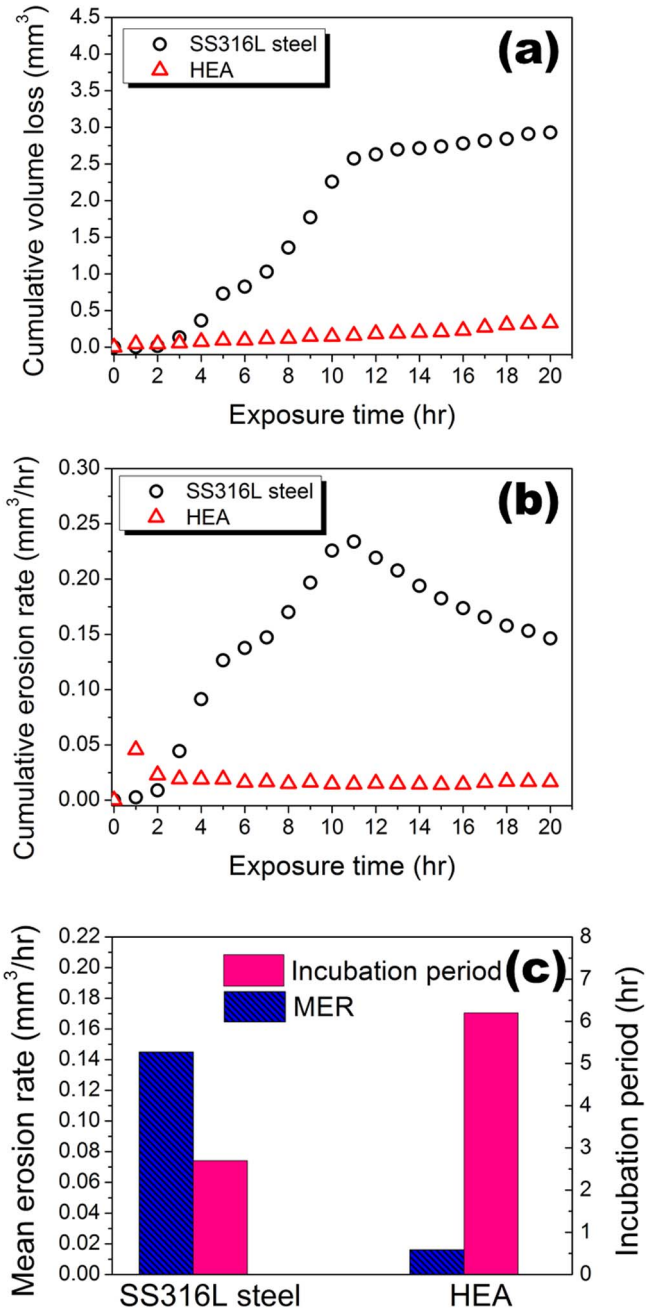

Fig. 5. (a) Cumulative volume loss, (b) cumulative erosion rate as a function of exposure time and (c) mean erosion rate and incubation period for $Al_{0.1}CrCoFeNi$ high entropy alloy (HEA) and SS316L stainless steel subjected to cavitation erosion testing in distilled water.

volume loss for HEA was almost one-tenth of that of the SS316L steel. After a small incubation period of 2.7 h a steep rise in volume loss was observed for SS316L steel. In contrast, the cumulative volume loss for the HEA showed a gradual increase with time. The incubation period for HEA was 2.3 times higher to that of the SS316L steel indicating high damage tolerance of the former. Fig. 5(b) and (c) shows the cumulative erosion rates and mean erosion rates for both the test materials. The mean erosion rates for HEA and SS316L were observed to be around 0.0166 mm^3/h and 0.1464 mm^3/h, respectively. The results indicate remarkably high cavitation erosion resistance of the HEA (around 9 times) compared to SS316L steel. It is interesting to observe that although the hardness and strength (yield and ultimate) for HEA are comparatively low (Table 2), it still showed better cavitation erosion resistance compared to stainless steel.

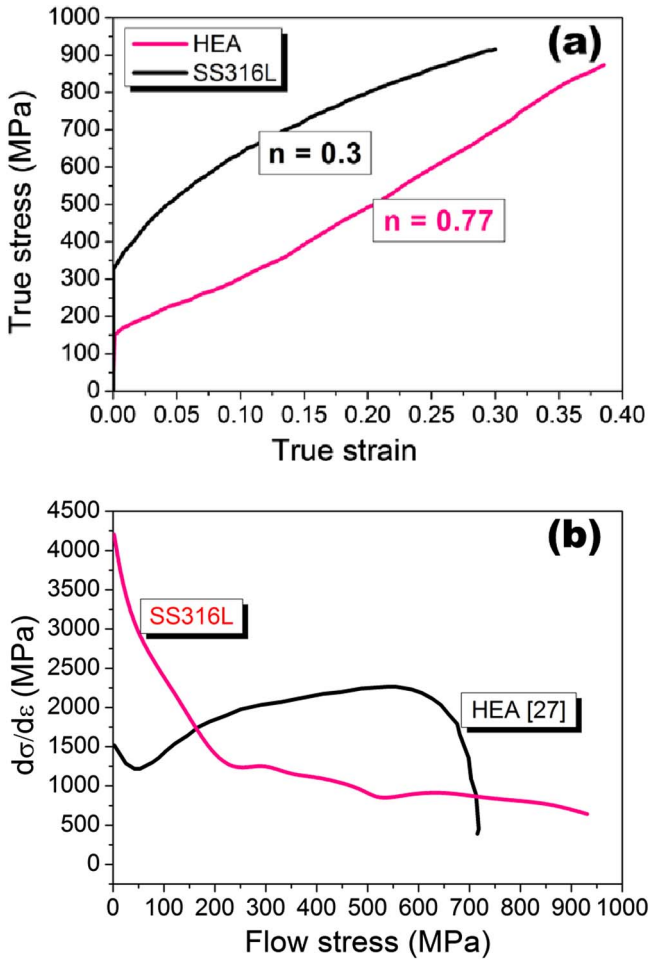

Fig. 6. (a) True stress-strain curves and (b) work-hardening rates for $Al_{0.1}CrCoFeNi$ high entropy alloy [27] (HEA) and SS316L stainless steel.

Generally, high hardness and strength are deemed to enhance the resistance to cavitation erosion [31,32]. Few previous studies showed the dependence of cavitation erosion behavior on the work-hardening and stacking fault energy of the material [33,34]. The work-hardening behavior for both the materials was analysed from the true stress-strain plots shown in Fig. 6(a). The work-hardening exponent (n) was calculated using the Hollomon's equation ($\sigma = K\varepsilon^n$) where σ is the true stress, K is the strength coefficient and ε is the true strain. The n value for HEA ($n = 0.77$) is significantly high compared to that of SS316L steel ($n = 0.3$). High n value for HEA indicates higher rate of increase in flow stresses as compared to SS316L steel which enhances the resistance to plastic deformation and thereby lowers the material removal rate.

Work-hardening behavior is related with the stacking fault energy (SFE) of the material. Zaddach et al. [35] reported that increasing the number of elements in equiatomic fraction alloys reduces the SFE. The decrease in SFE hinders the dissociation of partial dislocations and cross-slipping of dislocations leading to higher work hardening [36]. The SFE for the investigated HEA is not available, however, SFE for a similar composition HEA (CoCrFeNi) has been calculated to be around 17 mJ/m^2 [35]. Comparatively, SS316L steel has SFE of around 25 mJ/m^2 which contributed to its lower strain hardening exponent compared to that of the HEA. Work hardening rates for the two alloys are shown in Fig. 6(b). SS316 steel showed higher work-hardening rate in stage-I compared to HEA. This is followed by a continuous decrease in work-hardening rate as a function of flow stress for SS316L steel. Comparatively, the work-hardening rate of the HEA showed a significant increase in stage-II which continued over a significant range of flow stress. The enhanced work-hardening rate in stage-II for the HEA is believed to be due to formation of

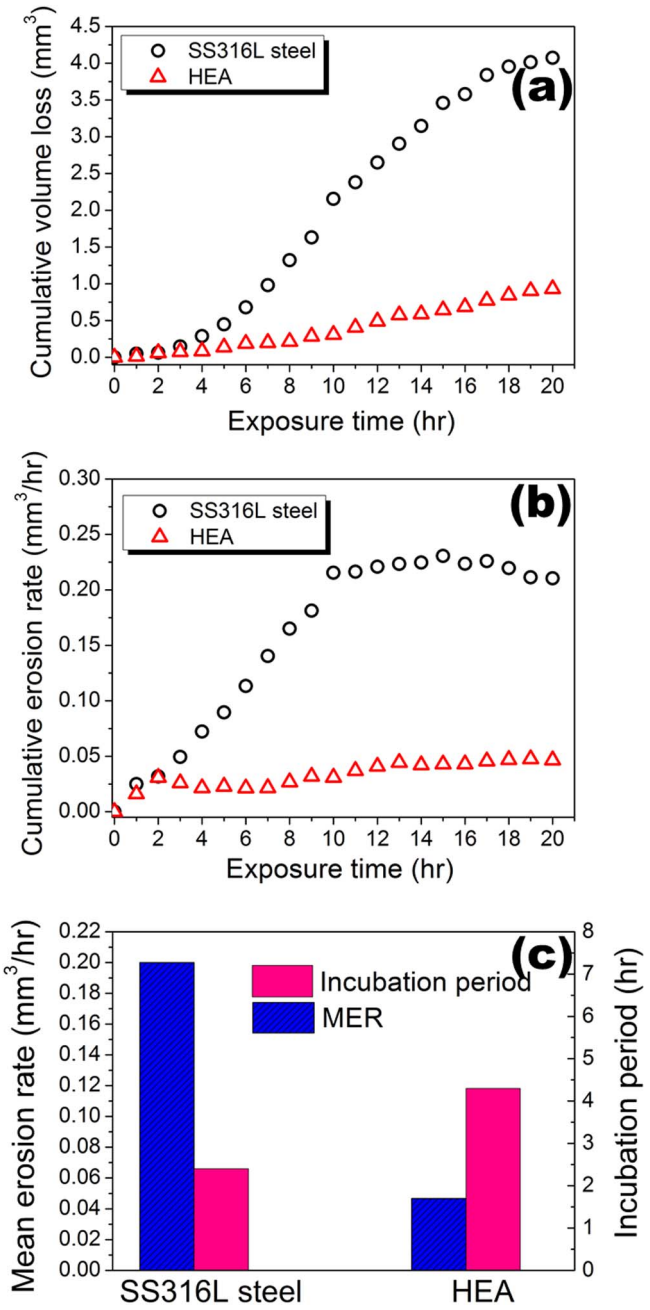

Fig. 7. (a) Cumulative volume loss, (b) cumulative erosion rate as a function of exposure time and (c) mean erosion rate and incubation period for $Al_{0.1}CrCoFeNi$ high entropy alloy (HEA) and SS316L stainless steel subjected to cavitation erosion-corrosion testing in distilled water containing 3.5 wt% NaCl.

nano-twins [30]. Further, cavitation erosion is a high strain rate deformation process involving impacts of high velocity micro-jets and shock waves. In general, flow stress increases with an increase in strain rate. The $Al_{0.1}CoCrFeNi$ HEA has been reported to demonstrate high value of strain rate sensitivity (m) compared to conventional FCC materials [37]. The increase in flow stress at high strain rates also contributes towards enhancing the cavitation erosion resistance. Thus, unusually high cavitation erosion resistance of the HEA may be partly attributed to its peculiar work-hardening behavior.

3.3. Cavitation erosion-corrosion behaviour

The Fig. 7(a) shows the cumulative volume loss of HEA and SS316L under cavitation erosion-corrosion condition. The cumulative volume loss under erosion-corrosion was higher for both the materials compared to pure erosion condition (Fig. 7a). Compared to SS316L steel, the HEA showed significant resistance to synergistic erosion-corrosion degradation. The mean erosion rate for HEA and SS316L was 0.046 mm^3/h and 0.2 mm^3/h, respectively (Fig. 7c). The cumulative volume loss for HEA after 20 h of testing was only 25% of that observed for SS316 steel resulting in four-fold higher resistance. Compared to higher incubation period for the HEA (6.5 h) under pure erosion condition, the incubation period in 3.5% NaCl solution was slightly lowered (4.3 h). The incubation period for SS316L steel under erosion-corrosion condition was also lowered. The decrease in incubation period may be the result of early removal of work-hardened layer due to corrosion.

Further, the CER in erosion-corrosion for SS316 steel was observed to increase continuously since the beginning of the test. Comparatively, a low and steady CER was observed for the HEA preceded by slightly high CER in the early stage. Near the completion of the test, the HEA showed significantly low and steady CER compared to high and unstable value of CER for the SS316L steel (Fig. 7b). It is further interesting to observe that HEA showed no appreciable difference in the shape of the CER curve with the change in test condition (pure erosion and erosion-corrosion) (Figs. 5b and 7b). In contrast, significant difference in the shape of CER curve was observed for SS316L steel with the change in test condition. HEA showed a deceleration stage in both erosion as well as in erosion-corrosion whereas, SS316L steel showed deceleration only for pure erosion condition but not for erosion-corrosion condition. This difference in the behavior for the two alloys may be attributed to difference in formation and removal of the work-hardened layer during erosion-corrosion. In pure erosion condition, both test materials showed deceleration stage due to work-hardening effect which effectively increases the flow stress. This behavior is consistent with the observed trend for other materials [32]. However, the work-hardened layer is likely to get removed by corrosion under erosion-corrosion condition. Therefore, the absence of deceleration stage for SS316L steel in erosion-corrosion condition may be related with continuous removal of the work-hardened layer through corrosion. In contrast, HEA with its high corrosion resistance limits the removal of work-hardened layer and showed higher erosion-corrosion resistance. HEAs are known to exhibit better corrosion resistance due to sluggish diffusion and cocktail effects [13]. Our recent study showed $Al_{0.1}CoCrFeNi$ HEA exhibits high activation energy and low mean jump rate compared to conventional materials contributing to its high

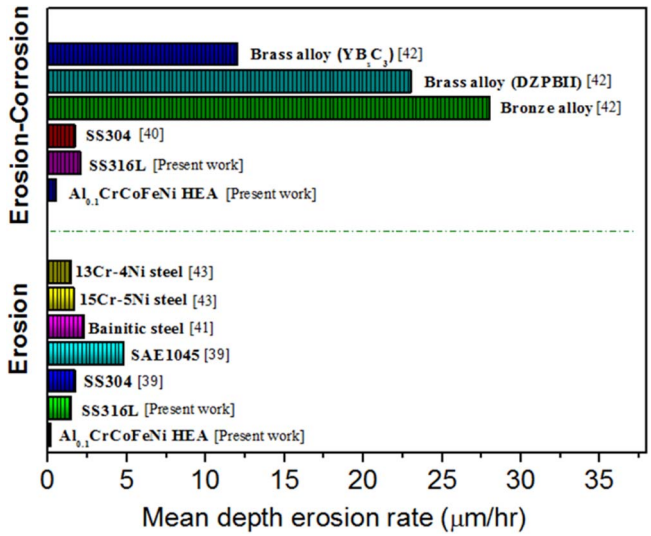

Fig. 8. Comparison of the mean depth erosion rates of the $Al_{0.1}CoCrFeNi$ high entropy alloy (HEA) with those of other structural materials [38–42] subjected to cavitation erosion and erosion-corrosion.

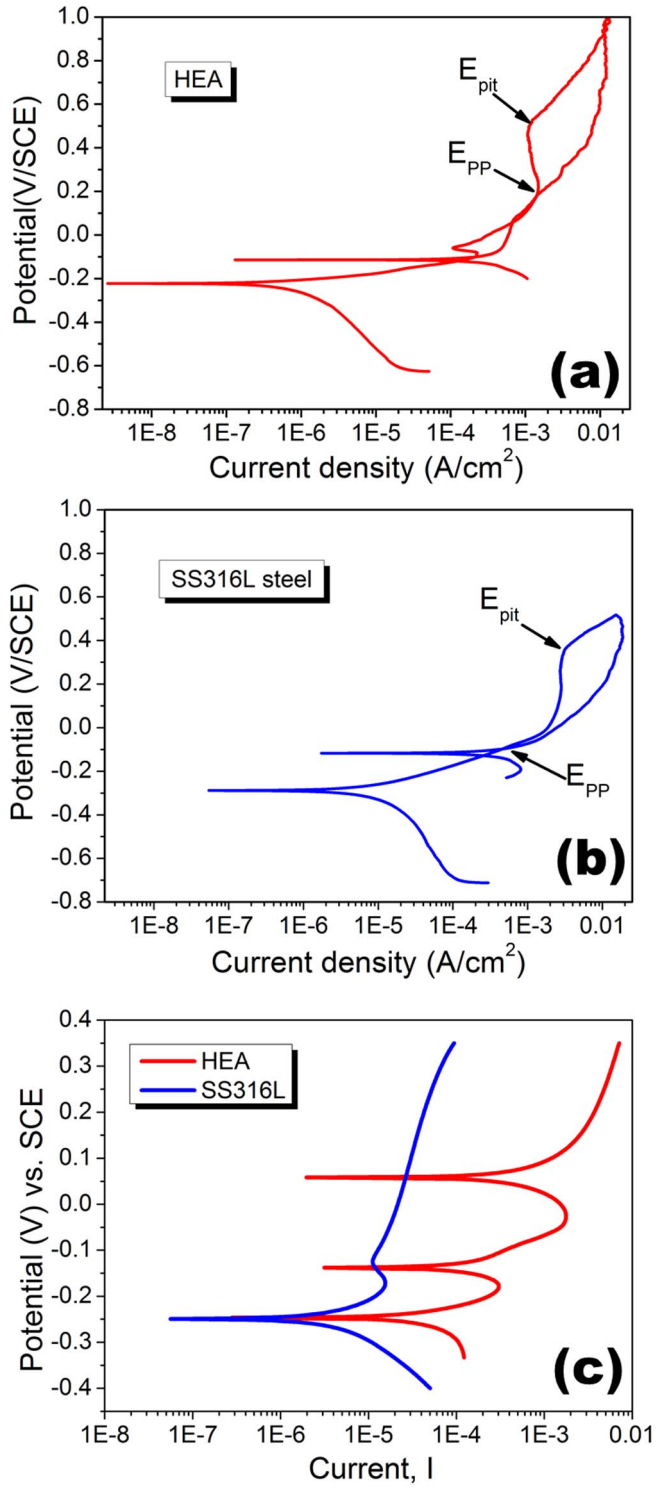

Fig. 9. Cyclic polarization testing results for (a) $Al_{0.1}CrCoFeNi$ high entropy alloy (HEA) and (b) SS316L stainless steel and (c) Intergranular corrosion results for the HEA and SS316L steel.

oxidation resistance and formation of stable oxide layer [19]. Further, a comparative analysis (Fig. 8) shows that $Al_{0.1}CoCrFeNi$ HEA exhibited significantly high degradation resistance under both erosion and erosion-corrosion conditions compared to different materials [38–42] highlighting its prominence as a potential structural materials under such conditions.

To further understand the effect of corrosion behavior on degradation of the test materials, standalone electrochemical corrosion studies were performed. The tafel and cyclic polarisation tests were conducted in 3.5 wt% NaCl solution for the both samples. The cathodic and anodic polarization curves obtained for HEA and SS316L are illustrated in Fig. 9. The corrosion current density (i_{corr}), corrosion potential (E_{corr}), pitting potential (E_{pit}) and protection potential (E_{pp}) calculated from tafel and cyclic polarization curves are summarized in Table 3. The corrosion rates for SS316L steel and the HEA calculated using Faraday's expression were around 4.65 mpy and 0.28 mpy, respectively. Significantly low corrosion rates for the HEA compared to SS316L steel highlights the superior corrosion resistance of the former. Further, compared to mean erosion rates in distilled water, the corrosion rates for the respective materials were significantly low indicating erosion-corrosion process to be erosion dominated. The HEA also showed higher pitting potential (E_{pit}) compared to SS316L steel (Fig. 9b). High values of pit initiation potential ($E_{pit} - E_{corr}$) and protection potential ($E_{pp} - E_{corr}$) indicates higher resistance to pit formation and propagation resulting in increase in passive layer stability. The HEA showed remarkable resistance to pit initiation and propagation compared to steel (Table 3). Furthermore, the loop area above E_{pp} representing the pitting severity was observed to be smaller for HEA (Table 3). The above results highlights the presence of stable passive film for HEA compared to SS316L steel. High stability of the passive layer for the HEA is attributed to the combined effect of high mixing entropy, sluggish diffusion and presence of passive layer forming elements such as Cr. The high mixing entropy decreases the free energy enhancing the system stability. Further, high mixing entropy impairs the diffusion process due to presence of low energy potential (LPE) lattice sites [43]. The LPE sites trap the atoms limiting the diffusion process. Additionally, $Al_{0.1}CrCoFeNi$ HEA forms single phase solid solution eliminating the chances for inter-granular corrosion due to the absence of secondary particles (Fig. 9c). Stainless steel shows a reactivation peak, signifying grain boundary sensitization, while there is no reactivation peak for the HEA. In stainless steel, the precipitation of carbides, particularly chromium carbides, along the grain boundaries makes the grain boundaries sensitized to localized attack. This is primarily attributed to the depletion of chromium along the grain boundaries, which is the principal element forming a stable passive layer in austenitic stainless steels. Thus, the combined effect of work-hardenability and high corrosion resistance resulted in enhanced cavitation erosion-corrosion resistance for the $Al_{0.1}CoCrFeNi$ HEA.

3.4. Material removal mechanism

Fig. 10 shows the surface morphology of degraded samples subjected to pure erosion and erosion-corrosion testing. Significant difference in the damage levels of both the samples on a macroscale can be observed (Fig. 10a and b). The surface of SS316L steel after 20 h of erosion-corrosion testing was covered with large macroscale pits.

Table 3
Comparative summary of electrochemical corrosion results for $Al_{0.1}CoCrFeNi$ high entropy alloy and stainless steel SS316L.

Material	I_{corr} (μA)	E_{corr} (mV)	E_{pit} (mV)	E_{pp} (mV)	$E_{pit} - E_{corr}$ (mV)	$E_{pp} - E_{corr}$ (mV)	Area under the loop (VA/cm^2)
$Al_{0.1}CoCrFeNi$ HEA	0.638	−225	490.3	184	715.3	409	5.38
SS316L	11.60	−289	359.8	−10.58	648.8	278.42	6.48

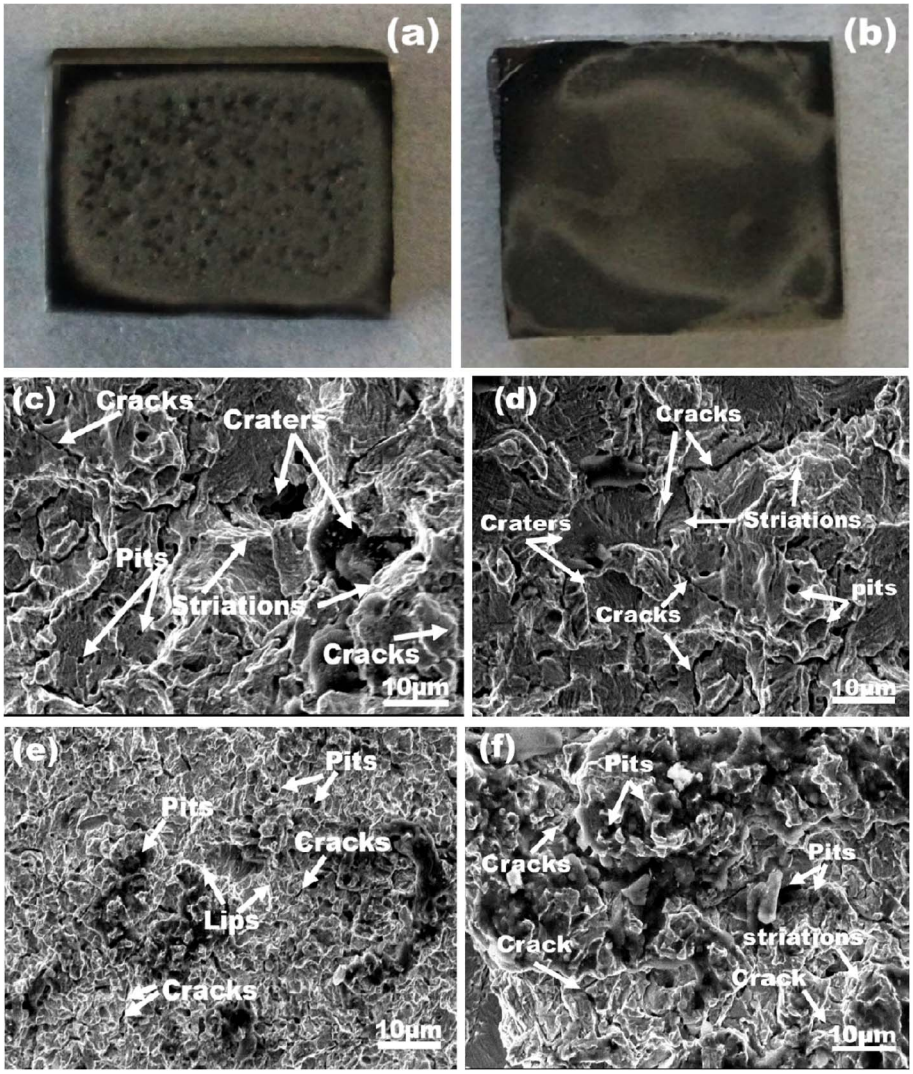

Fig. 10. Macrographs showing the (a) SS316L steel and (b) $Al_{0.1}CrCoFeNi$ high entropy alloy (HEA) samples subjected to cavitation erosion-corrosion testing for 20 h. The scanning electron microscope (SEM) images showing surface morphology of SS316L steel tested under (c) cavitation erosion and (d) cavitation erosion-corrosion after 20 h. The SEM images showing surface morphology of $Al_{0.1}CrCoFeNi$ HEA tested under (e) cavitation erosion and (f) cavitation erosion-corrosion after 20 h.

Comparatively, the surface of HEA subjected to similar test conditions was free of such macroscale pits. Both HEA and SS316L show ductile material removal mode with signs of plastic deformations and fatigue (Fig. 10). No significant difference was observed in surface morphologies of the samples subjected to pure erosion and erosion-corrosion for both the materials. Under both the test conditions, degraded surfaces were composed of deep pits and cracks. However, difference in severity of deformation is evident for the two test materials. The surface of SS316L steel was covered with large craters and large number of deep pits (Fig. 10c and d). In case of the HEA, pits and cracks were significantly small in size (Fig. 10e and f). Further, large craters as observed for SS316L steel were not detected for the HEA. Comparison of the SEM images clearly indicates significant deterioration of SS316L steel compared to the HEA. These results are in agreement with the trend observed in CER for these materials. The small sized pits and cracks for HEA are related with its high work hardening behavior. Microhardness measured along the depth of the cross-sectioned eroded samples is shown in Fig. 11. Results showed an increase in hardness for both the test materials, however, the HEA showed more than two-fold increase compared to 1.27 times for SS316L steel. The XRD analysis of the post-eroded samples (Fig. 12) showed presence of strain-induced martensite for the SS316L steel and FCC to BCC transition for the HEA. These microstructural changes during the erosion process can contribute towards increased hardness. Further, the significant increase in sub-surface hardness for the HEA also relates to its high work-hardenability as also observed from the stress-strain plots (Fig. 6). Work-hardening increases the flow stress required for plastic deformation and initiation of pits. The optical micrographs of the eroded samples (inset Fig. 11) show severely deformed microstructure beneath the eroded surface for the SS316L steel while no such deformation is visible for the

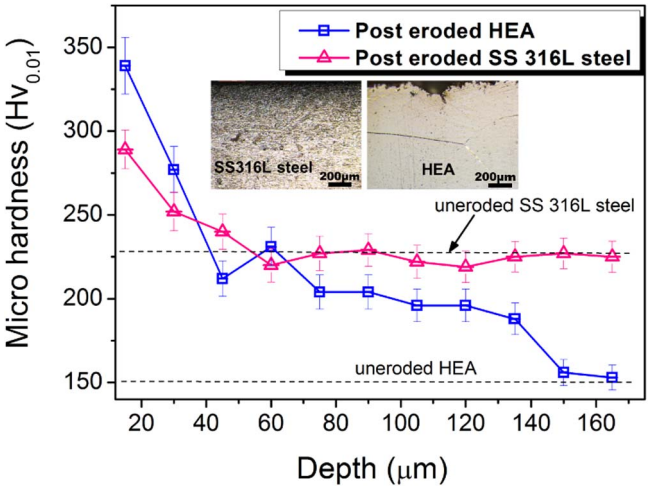

Fig. 11. Variation in sub-surface microhardness of the SS316L stainless steel and $Al_{0.1}CoCrFeNi$ high entropy alloy (HEA) subjected to cavitation erosion testing. Insets show the optical microscopy images of the sub-surface microstructure.

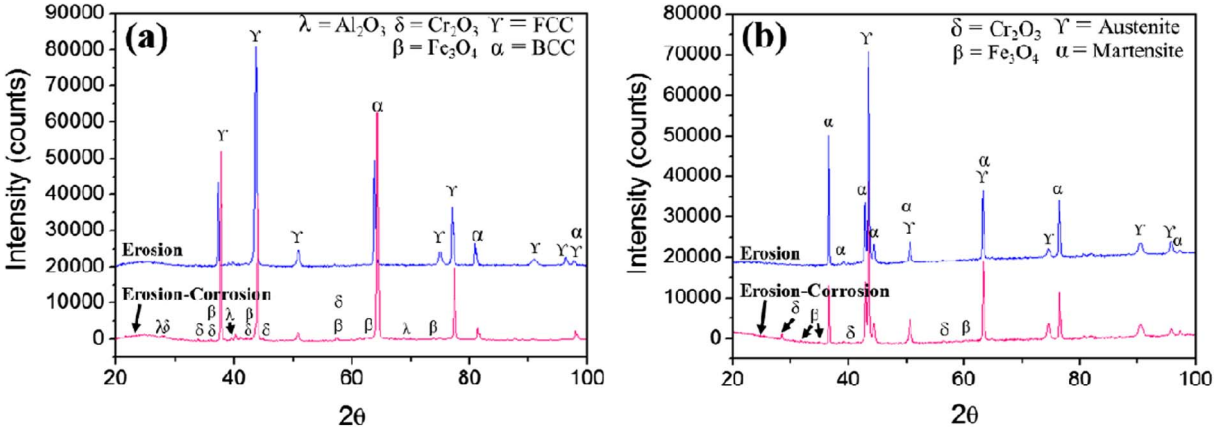

Fig. 12. X-ray diffraction results of the (a) $Al_{0.1}$CoCrFeNi high entropy alloy (HEA) and (b) SS316L stainless steel after cavitation erosion and erosion-corrosion.

HEA. Insignificant change in the microstructure (at the observed length scale) for the HEA post testing could be explained on the basis of its work-hardening through nanoscale twining [28]. Furthermore, the $Al_{0.1}$CrCoFeNi HEA also showed high strain rate sensitivity [37] which also enhances the flow stress due to increased dislocation intersections. Increased flow stress for the HEA due to work hardening hinders plastic deformation due to impact of high velocity micro jets. As a results, the size of pits observed for HEA were significantly small compared to SS316L steel.

Further, the XRD analysis of the samples subjected to erosion-corrosion testing showed presence of different oxides which may have contributed to the corrosion process. Both materials showed presence of chromium (III) oxide along with that of Fe3O4. In addition, the presence of α-Al2O3 was also observed for the HEA. Both Cr2O3 and Al2O3 are known to be highly protective in nature, limiting the corrosion of the underlying material. Compared to the SS316L steel, presence of Al2O3 might also have restricted the corrosion and passive layer thickness by limiting iron diffusion. Al2O3 is known to possess lower free energy compared to Cr2O3 and Fe3O4 which will likely facilitate rapid formation of the passive layer on the HEA. Owing to high passivation kinetics of the HEA, the diffusion of ions would be limited lowering the corrosion rates. Further, the evolution of strain-induced martensite in SS316L steel, enhances its susceptibility to intergranular corrosion through formation of micro galvanic-cells. Additionally, density of the grain-boundaries is significantly lower in HEA compared to SS316L steel due to large sized grains. The grain boundaries can act as a passage for diffusion of ion. Thus, low grain boundary density for the HEA might have also restricted the ion diffusion lowering the corrosion rates. Thus, the combined effect of toughness and work-hardening along with tendency to form stable passive film helped enhance the cavitation erosion-corrosion resistance of the $Al_{0.1}$CrCoFeNi HEA compared to SS316L steel.

4. Conclusion

We investigated the cavitation erosion and corrosion behavior of the $Al_{0.1}$CoCrFeNi high entropy alloy (HEA) using ultrasonication technique. For comparison, conventionally used SS316L stainless steel was also evaluated in identical experimental conditions. Compared to SS316L steel, the HEA showed significantly higher resistance to pure erosion (around nine times) as well as erosion-corrosion (around four times) in terms of mean erosion rate. The HEA also showed longer incubation period compared to SS316L steel. The superior performance of HEA compared to SS316L steel was attributed to the increased work-hardening of the former. Both the work-hardening exponent and strain rate sensitivity were higher for the HEA. Further, the HEA also showed significant work-hardening rate over a large range of flow stress in second stage. Electrochemical corrosion testing showed high pitting resistance and protection potential leading to much lower corrosion rates with formation of stable passive film. The SS316L steel showed substantial intergranular corrosion compared to the HEA. Thus, the combined effect of high work-hardening and better corrosion resistance resulted in improved cavitation erosion-corrosion resistance. Therefore, $Al_{0.1}$CoCrFeNi HEA is a promising structural material for protection against cavitation erosion and corrosion.

References

[1] G. Stachowiak, A.W. Batchelor, Engineering Tribology, Butterworth-Heinemann, 2013.
[2] J.P. Franc, J.M. Michel, Fundamentals of Cavitation, Kluwer Academic Publishers, 2004.
[3] C. Kwok, F. Cheng, H. Man, Synergistic effect of cavitation erosion and corrosion of various engineering alloys in 3.5% NaCl solution, Mater. Sci. Eng. A 290 (2000) 145–154.
[4] S. Hong, Y. Wu, J. Zhang, Y. Zheng, Y. Zheng, J. Lin, Synergistic effect of ultrasonic cavitation erosion and corrosion of WC–CoCr and FeCrSiBMn coatings prepared by HVOF spraying, Ultrason. Sonochem. 31 (2016) 563–569.
[5] L. Qiao, Y. Wu, S. Hong, J. Zhang, W. Shi, Y. Zheng, Relationships between spray parameters, microstructures and ultrasonic cavitation erosion behavior of HVOF sprayed Fe-based amorphous/nanocrystalline coatings, Ultrason. Sonochem. 39 (2017) 39–46.
[6] B. Vyas, I.L. Hansson, The cavitation erosion-corrosion of stainless steel, Corros. Sci. 30 (1990) 761–770.
[7] I. Mitelea, E. Dimian, I. Bordeaşu, C. Crăciunescu, Ultrasonic cavitation erosion of gas nitrided Ti–6Al–4V alloys, Ultrason. Sonochem. 21 (2014) 1544–1548.
[8] R. Menon, Cavitation resistant alloy for hydroturbine repair, ASCE, Atlanta, GA, USA, 1997, pp. 1087–1093.
[9] C.T. Kwok, H.C. Man, F.T. Cheng, Cavitation erosion of duplex and super duplex stainless steels, Scripta Mater. 39 (1998) 1229–1236.
[10] B. Cantor, I. Chang, P. Knight, A. Vincent, Microstructural development in equiatomic multicomponent alloys, Mater. Sci. Eng. A 375 (2004) 213–218.
[11] M.-H. Tsai, J.-W. Yeh, High-entropy alloys: a critical review, Mater. Res. Lett. 2 (2014) 107–123.
[12] J.W. Yeh, S.K. Chen, S.J. Lin, J.Y. Gan, T.S. Chin, T.T. Shun, C.H. Tsau, S.Y. Chang, Nanostructured high-entropy alloys with multiple principal elements: novel alloy design concepts and outcomes, Adv. Eng. Mater. 6 (2004) 299–303.
[13] B. Murty, J.-W. Yeh, S. Ranganathan, High-entropy Alloys, Butterworth-Heinemann, 2014.
[14] J.-M. Wu, S.-J. Lin, J.-W. Yeh, S.-K. Chen, Y.-S. Huang, H.-C. Chen, Adhesive wear behavior of AlxCoCrCuFeNi high-entropy alloys as a function of aluminum content, Wear 261 (2006) 513–519.
[15] C. Lee, C. Chang, Y. Chen, J. Yeh, H. Shih, Effect of the aluminium content of $Al_xCrFe_{1.5}MnNi_{0.5}$ high-entropy alloys on the corrosion behaviour in aqueous environments, Corros. Sci. 50 (2008) 2053–2060.
[16] M.-H. Chuang, M.-H. Tsai, W.-R. Wang, S.-J. Lin, J.-W. Yeh, Microstructure and wear behavior of $Al_xCo_{1.5}CrFeNi_{1.5}$Tiy high-entropy alloys, Acta Mater. 59 (2011) 6308–6317.
[17] J.H. Zhao, X.L. Ji, Y.P. Shan, Y. Fu, Z. Yao, On the microstructure and erosion–corrosion resistance of AlCrFeCoNiCu high-entropy alloy via annealing treatment, Mater. Sci. Technol. (2016) 1–5.
[18] C. Lee, Y. Chen, C. Hsu, J. Yeh, H. Shih, Enhancing pitting corrosion resistance of $Al_xCrFe_{1.5}MnNi_{0.5}$ high-entropy alloys by anodic treatment in sulfuric acid, Thin Solid Films 517 (2008) 1301–1305.
[19] H.S. Grewal, R.M. Sanjiv, H.S. Arora, R. Kumar, A. Ayyagari, S. Mukherjee, H. Singh, Activation energy and high temperature oxidation behavior of multi-principal element alloy, Adv. Eng. Mater. (2017) e201700182-n/a.

[20] Y. Wang, B. Li, M. Ren, C. Yang, H. Fu, Microstructure and compressive properties of AlCrFeCoNi high entropy alloy, Mater. Sci. Eng. A 491 (2008) 154–158.
[21] W.-R. Wang, W.-L. Wang, S.-C. Wang, Y.-C. Tsai, C.-H. Lai, J.-W. Yeh, Effects of Al addition on the microstructure and mechanical property of Al_xCoCrFeNi high-entropy alloys, Intermetallics 26 (2012) 44–51.
[22] T.-T. Shun, C.-H. Hung, C.-F. Lee, The effects of secondary elemental Mo or Ti addition in $Al_{0.3}$CoCrFeNi high-entropy alloy on age hardening at 700 C, J. Alloy. Compd. 495 (2010) 55–58.
[23] C.-M. Lin, H.-L. Tsai, Evolution of microstructure, hardness, and corrosion properties of high-entropy Al 0.5 CoCrFeNi alloy, Intermetallics 19 (2011) 288–294.
[24] Q. Tang, Y. Huang, H. Cheng, X. Liao, T.G. Langdon, P. Dai, The effect of grain size on the annealing-induced phase transformation in an $Al_{0.3}$CoCrFeNi high entropy alloy, Mater. Des. 105 (2016) 381–385.
[25] C. Wu, S. Zhang, C. Zhang, H. Zhang, S. Dong, Phase evolution and cavitation erosion-corrosion behavior of FeCoCrAlNiTi_x high entropy alloy coatings on 304 stainless steel by laser surface alloying, J. Alloy. Compd. 698 (2017) 761–770.
[26] S. Zhang, C. Wu, C. Zhang, M. Guan, J. Tan, Laser surface alloying of FeCoCrAlNi high-entropy alloy on 304 stainless steel to enhance corrosion and cavitation erosion resistance, Opt. Laser Technol. 84 (2016) 23–31.
[27] Y. Shi, B. Yang, X. Xie, J. Brechtl, K.A. Dahmen, P.K. Liaw, Corrosion of Al_xCoCrFeNi high-entropy alloys: Al-content and potential scan-rate dependent pitting behavior, Corros. Sci. (2017).
[28] M. Komarasamy, N. Kumar, Z. Tang, R. Mishra, P. Liaw, Effect of microstructure on the deformation mechanism of friction stir-processed Al0. 1CoCrFeNi high entropy alloy, Mater. Res. Lett. 3 (2015) 30–34.
[29] F. Otto, Y. Yang, H. Bei, E.P. George, Relative effects of enthalpy and entropy on the phase stability of equiatomic high-entropy alloys, Acta Mater. 61 (2013) 2628–2638.
[30] N. Kumar, M. Komarasamy, P. Nelaturu, Z. Tang, P.K. Liaw, R.S. Mishra, Friction stir processing of a high entropy alloy $Al_{0.1}$CoCrFeNi, JOM 67 (2015) 1007–1013.
[31] C.T. Kwok, F.T. Cheng, H.C. Man, Laser surface modification of UNS S31603 stainless steel using NiCrSiB alloy for enhancing cavitation erosion resistance, Surf. Coat. Technol. 107 (1998) 31–40.
[32] A. Karimi, J.L. Martin, Cavitation erosion of metals, Int. Met. Rev. 31 (1986) 1–26.
[33] X.-F. Zhang, L. Fang, The effect of stacking fault energy on the cavitation erosion resistance of [alpha]-phase aluminum bronzes, Wear 253 (2002) 1105–1110.
[34] R.H. Richman, W.P. McNaughton, Correlation of cavitation erosion behavior with mechanical properties of metals, Wear 140 (1990) 63–82.
[35] A.J. Zaddach, C. Niu, C.C. Koch, D.L. Irving, Mechanical properties and stacking fault energies of NiFeCrCoMn high-entropy alloy, JOM 65 (2013) 1780–1789.
[36] G.E. Dieter, D.J. Bacon, Mechanical Metallurgy, McGraw-Hill, London, New York, 1988.
[37] M. Komarasamy, N. Kumar, R.S. Mishra, P.K. Liaw, Anomalies in the deformation mechanism and kinetics of coarse-grained high entropy alloy, Mater. Sci. Eng. A 654 (2016) 256–263.
[38] M.G. Di, V. Cuppari, R.M. Souza, A. Sinatora, Effect of hard second phase on cavitation erosion of Fe-Cr-Ni-C alloys, Wear 258 (2005) 596–603.
[39] C.L. Wu, S. Zhang, C.H. Zhang, H. Zhang, S.Y. Dong, Phase evolution and cavitation erosion-corrosion behavior of FeCoCrAlNiTi_x high entropy alloy coatings on 304 stainless steel by laser surface alloying, J. Alloy. Compd. 698 (2017) 761–770.
[40] G.B. Jiang, Y.K. Zheng, Y.Y. Yang, H.S. Fang, Cavitation erosion of bainitic steel, Wear 215 (1998) 46–53.
[41] A. Sakamoto, H. Funaki, M. Matsumura, Influence of galvanic macro-cell corrosion on the cavitation erosion durability assessment of metallic materials–International cavitation erosion test of Gdansk, Wear 186–187 (1995) 542–547.
[42] G. Taillon, F. Pougoum, S. Lavigne, L. Ton-That, R. Schulz, E. Bousser, S. Savoie, L. Martinu, J.-E. Klemberg-Sapieha, Cavitation erosion mechanisms in stainless steels and in composite metal–ceramic HVOF coatings, Wear 364 (2016) 201–210.
[43] K.Y. Tsai, M.H. Tsai, J.W. Yeh, Sluggish diffusion in Co-Cr-Fe-Mn-Ni high-entropy alloys, Acta Mater. 61 (2013) 4887–4897.